Title

Catechol redox maintenance in mussel adhesion

Authors

Wang, Stephanie X

Waite, J Herbert

Publication Date

2025-01-15

DOI

10.1038/s41570-024-00673-4

nature reviews chemistry

https://doi.org/10.1038/s41570-024-00673-4

Review article

Check for updates

Catechol redox maintenance in mussel adhesion

Stephanie X. Wang [1] & J. Herbert Waite [1,2]

Abstract

Catechol-functionalized proteins in mussel holdfasts are essential for underwater adhesion and cohesion and have inspired countless synthetic polymeric materials and devices. However, as catechols are prone to oxidation, long-term performance and stability of these inventions awaits effective antioxidation strategies. In mussels, catechol-mediated interactions are stabilized by 'built-in' homeostatic redox reservoirs that restore catechols oxidized to quinones. Mussel byssus has a typical 'core-shell' architecture in which the core is a degradable fibrous block copolymer consisting of collagen and fibroin coated by robust protein networks stabilized by bis-catecholato-metal and tris-catecholato-metal ion complexes. The coating is well-adapted to protect the core against abrasion, hydrolysis and microbial attack, but it is not impervious to oxidative damage, which, during function, is promptly repaired by redox poise via coacervated catechol-rich and thiol-rich reducing interlayers and inclusions. However, when the e^- and H^+ equivalents from these reducing reservoirs are depleted, coating damage accumulates, leading to exposure of the vulnerable core to environmental attack. Heeding and translating these strategies is essential for deploying catechols with longer service lifetimes and designing more sustainable next-generation polymeric adhesives.

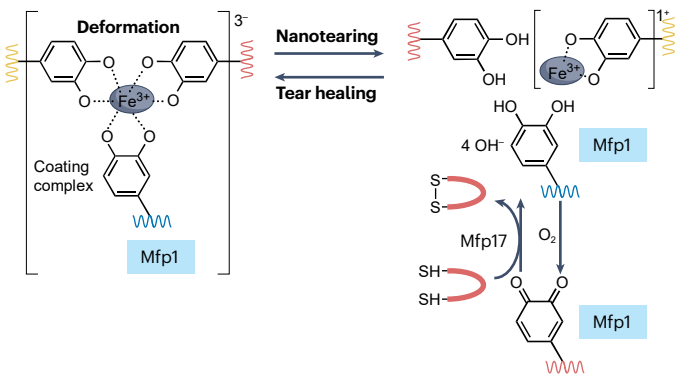

[1]Department of Chemistry & Biochemistry, University of California Santa Barbara, Santa Barbara, CA, USA. [2]Department of Molecular, Cell & Developmental Biology, University of California Santa Barbara, Santa Barbara, CA, USA. e-mail: hwaite@ucsb.edu

Introduction

The interfacial landscape between an adhesive protein and its binding surface is as changeable as the ambient environment. Anchored or sessile aquatic organisms have a default palette of 20 different canonical amino acid functionalities to adapt their adhesive proteins to surfaces, but this is not always adequate. A supplementary orthogonal system of adaptation involving a diverse array of enzyme-catalysed post-translational amino acid modifications[1] can be used for special challenges. Catechol (which is another name for *o*-dihydroxybenzene) functionalities are notable examples of this, and they are used by a variety of organisms to enhance opportunistic underwater protein-mediated adhesion and cohesion. The first report of catecholic side chains in an adhesive protein of mussel byssus[2] spurred numerous efforts to capture and translate this motif for diverse synthetic applications. The range and variety of mussel-inspired applications beyond underwater adhesives[3] is vast — from self-healing punctures[4] to graphene oxide composites[5], calvarial bone cement[6] and coatings for CO_2 capture[7], to mention a few. Given catechol susceptibility to oxidation, however, a profitable long-term capture of catecholic attributes as durable as those in mussels has proven elusive in aerobic environments. Two important translational breakthroughs using catechol-functionalized polymers underscore this limitation: the first described a spontaneously self-healing hydrogel[8], the second, a resin[9] that combined high stiffness with high extensibility. Despite their astonishing prowess, the critical properties of these materials were short-lived (~24 h) due to catechol oxidation — a vulnerability that haunts most catechol-inspired translations. Two remedies to reduce catechol susceptibility to oxidation have been proposed: either functionalizing polymers with catecholic analogues, such as 2,3-dihydroxybenzoic acid[10] and 3-hydroxy-4-pyridinone[11], among others[12], that are less prone to oxidation, or reformulating catechol-functionalized polymeric materials so that the desired redox state is maintained by redox poise — a balanced distribution of electron-carrying intermediates in both their oxidized and reduced states[13,14]. Relying on redox poise is the strategy used by mussels, and it offers scope for substantive and sustainable innovation in science and technology.

Not unlike single-use consumer products, mussel byssal threads, long cylindrical fibres tipped by spatulate plaques, are mass-produced to adhere instantly to hard wet surfaces in turbulent intertidal zones[15] (Fig. 1a). Depending on a mussel's age, each thread takes a mussel between 0.5 and 5 min to make, and, in adults, it has a service life of at least ~9 weeks before being jettisoned[16]. Full details of byssus formation have been covered elsewhere[15,17,18]. Thread production capacity can reach ~600 threads per month per mussel and is dictated by prevailing seasonal conditions[19]. With a maximum life expectancy of 50–100 years[20], a single mussel (*Mytilus californianus*) could produce and discard up to 6×10^5 threads in a lifetime. To avoid suffocation by their own byssal rubbish, mussel colonies count on thread embrittlement and aggressive ambient microbial proteases[21–23] for timely degradation. Recapture of byssal rubbish-derived nutrients by filter-feeding mussels would enhance the survival value of this system.

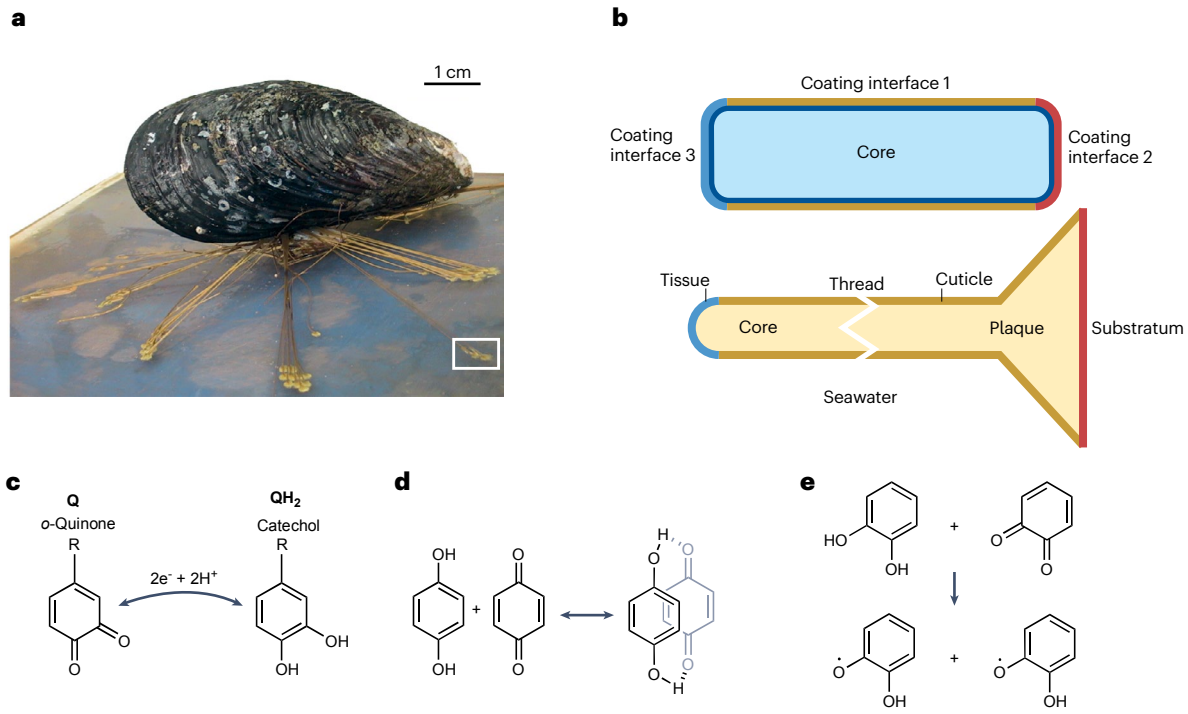

Fig. 1 | Mussels, byssal threads and catechol/quinone redox partners. **a**, A mussel, *Mytilus californianus*, attached by a byssus, a holdfast of radially distributed threads tipped with plaques, to a glass plate. **b**, Comparing a byssal thread with the core-shell material design. The shell or coating faces the local ambient environment whereas the core is in the interior covered and protected by the coating, which is often multilayered. In byssus, local ambient environments are seawater, substratum for adhesion and/or living tissue. **c**, A substituted catechol or 3,4-dihydroxybenzene, with substitution at R, occurs throughout nature and readily undergoes oxidation to an *o*-quinone. In mussel foot proteins, the catecholic moiety of the amino acid 3,4-dihydroxyphenyl-L-alanine has R = -$CH_2CH(NH_3^+)$-COO^-. **d**,**e**, Quinones are unstable and form diverse products, but initial products can include stacked quinhydrones (shown here as the *p*-hydroquinone) (part **d**), and free-radical semiquinones (part **e**).

Balancing thread function with obsolescence is a tricky business that relies equally on catechol redox control and thread architecture. Like an increasing number of natural materials[24], byssal threads follow a common design blueprint called 'core-shell' that consists of packaging core components within layered 'shells' or coatings[25] (Fig. 1b). The degradable core provides threads with essential mechanical properties, such as stiffness, cohesive strength, energy dissipation and more, whereas the more robust catechol-rich coating, which faces the ambient environment, protects the core against environmental degradation. The coating can be adapted to face more than one environment and does so in byssus, facing the substratum, living tissue and ambient seawater[26] (Fig. 1b). If, at some point during service, catechol oxidation in the coating exceeds the capacity for repair, the damaged thread is allowed to fail and is replaced by a new thread.

This Review discusses how the homeostasis between catechol redox and dynamic mechanochemistry enables function and obsolescence in byssal threads. Research conducted over the past 10–15 years has established that byssal adhesion and cohesion are dominated by an extensive network of catechol-functionalized proteins coordinated with metal ions such as Fe^{3+}, V^{+3} and Al^{3+}, as well as metal oxides[14,27,28]. Although catechol redox is passivated by coordination, under tension following ligand–metal bond rupture, catechols become prone to oxidation. The role of redox homeostasis in maintaining catechols during cyclic structural deformation is not widely appreciated and merits description for better concept capture and translation. The 'robust shell-degradable core' architecture of byssus also offers insights for a sustainable redesign of human single-use consumer products.

Dealing with catechols

In the sections below, we describe the context of catechol use in nature, catechol instability to oxidation, strategies to curb instability and methods to measure redox tendencies.

Catecholic biomacromolecules

Living organisms have a longstanding partiality towards redox-active catechols, also known as *o*-dihydroxybenzenes and *o*-hydroquinones, for diverse essential biomacromolecules, including lignins[29], siderophores[30], melanins[31] and exoskeletal sclerotins[32]. Catechol partiality is hardly surprising, given the number of interactions that catechols are exceptionally good at, including hydrogen bonding, surface dehydration, metal coordination, Michael additions and phenol coupling reactions, among others that have been well-covered in reviews[33–36]. A reliance on catechols, however, also requires exquisite redox control, given how prone catechols are to oxidation. Before exploring the role of catechol maintenance in mussel byssal threads, we detail three points: how catechol instability is linked to its redox potential E'_o; how catechol redox is influenced by other redox systems, pH and stoichiometry; and how catechol redox is investigated in mussel byssus.

Catechol redox

Catechol (QH_2) rarely, if ever, occurs without its *o*-quinone (Q) counterpart. The simple redox half-reaction with a standard hydrogen electrode (SHE) relating Q and QH_2 in the case of 3,4-dihydroxyphenyl-L-alanine (Dopa)[37], a catecholic amino acid, is:

$$Q + 2e^- + 2H^+ \rightarrow QH_2 \; E_o = +0.25\ V\ (pH\ 7\ and\ 25\ °C)\ SHE.\ Half-reaction\ a$$

The chemical structures are shown in Fig. 1c. By convention in formal half-reactions, which are usually assumed to be reversible, Q or the 'oxidized' form, is on the left under the following conditions: 1 M Q and QH_2, 1 atm, 25 °C, pH 7 and pure water as solvent[38]. In picking up $2e^-$ and $2H^+$, Q is 'reduced' to QH_2 (right). A positive formal redox potential E'_o implies that, under the stated conditions, Q seeks $2e^-$ and $2H^+$ more avidly than QH_2 surrenders them. Dopa redox was selected as a convenient representative for the catechol in byssus proteins, but redox potentials are quite wide-ranging for catechols, especially when influenced by side chain electron-withdrawing tendencies[10,12,39].

Table 1 | Formal redox potentials of half-reactions relevant to catechol chemistry. Ag/AgCl potentials (E'_o Ag/AgCl) are added for comparison

Half-reactions (pH 7; 25 °C)	E'_o SHE (V)	E'_o Ag/AgCl (V)	Ref.
$½\,O_2 + 2H^+ + 2e^- \longrightarrow H_2O$	+0.816	+0.619	38
$½\,O_2 + H_2O + 2e^- \longrightarrow H_2O_2$	+0.300	+0.103	38
$Q + 2H^+ + 2e^- \longrightarrow QH_2$ (Dopa)	+0.333	+0.135	37
$R\text{-}S\text{-}S\text{-}R' + 2H^+ + 2e^- \longrightarrow 2Cys\text{-}SH$	−0.220	−0.417	38
$DPPH^{\cdot} + H^+ + e^- \longrightarrow DPPH\text{-}H$	+0.540	+0.343	49

Dopa, 3,4-dihydroxyphenyl-L-alanine; $DPPH^{\cdot}$, 2,2-diphenyl-1-picrylhydrazyl free radical; E'_o, redox potential; Q, *o*-quinone; QH_2, catechol; SHE, standard hydrogen electrode.

As written, Half-reaction a reveals little about the complexity of $Q–QH_2$ relationships. Even under an inert gas over an electrode surface, Half-reaction a rapidly loses reversibility. Two well-known contributors to this are quinhydrone formation and comproportionation (Fig. 1d,e). Quinhydrone is a peculiar noncovalent complex of paired product and reactant ($Q–QH_2$) mutually stabilized by H-bonds and π-stacking[40], whereas, in comproportionation[41], a one-electron transfer takes place from QH_2 to Q, resulting in two semiquinones or $2QH^{\cdot}$, which commonly undergo further covalent phenol coupling[42] and other free-radical formations as in the Fenton reaction[43].

Coupling catechol redox

The $Q–QH_2$ redox in Half-reaction a is meaningless without a coupled half-reaction for context. Table 1 lists a few half-reactions often coupled with catechol — two examples are adequate for demonstrating the influence of context. The first example is the reduction of oxygen to water (Half-reaction b) in seawater (20 °C), with a typical oxygen concentration of ~250 μM[44]. In principle, this can be combined with Half-reaction a to estimate a net $\Delta E'_o$. In this case, QH_2 (left) submits electrons and protons to the dominant oxidant O_2, which is reduced to water. As the electron and proton exchange in the two half-reactions must be balanced, the less positive half-reaction is subtracted from the more positive one (Reaction 1):

$$QH_2 \rightarrow Q + 2e^- + 2H^+ \; (E'_o = +0.25\ V)\ Half-reaction\ a$$
$$1/2O_2 \pm 2e^- \pm 2H^+ \rightarrow H_2O \; (E'_o = +0.82\ V)\ Half-reaction\ b$$
$$1/2O_2 + QH_2 \rightarrow H_2O + Q \; (\Delta E'_o = +0.57\ V)\ Reaction\ 1$$

Again, redox reactions here are less than revealing about their chemical limitations. Due to a high energy of activation, triplet O_2 strongly resists reduction, but this is readily overcome by catalytic trace metals, particularly soluble iron and copper complexes (refs. 45,46), which are pervasive in all biological media, including seawater.

The second example of coupled half-reactions combines thiol oxidation with Q reduction (Reaction 2), assuming solvent-accessible protein cysteinyl thiols. This time, because Half-reaction a has a more positive redox potential than the disulfide reduction, Q reduction will

prevail and acquire its electrons from two R-SH groups. It goes without saying that the disulfide and thiol redox potentials, like those of substituted catechols, can range beyond the representative E'_o used here. Subtracting Half-reaction c from Half-reaction a reveals that thiols spontaneously restore Q to QH_2. Detailed studies of Reaction 2 indicate that Cys thiols form transient covalent Cys-S–Dopa adducts that do not accumulate until the 2:1 thiol:Q stoichiometry wanes[47].

$$Q + 2e^- + 2H^+ \rightarrow QH_2\ (E_o = +0.25\ V)\ \text{Half-reaction a}$$
$$2RSH \rightarrow RS-SR \pm 2e^- \pm 2H^+\ (E_o = -0.22\ V)\ \text{Half-reaction c}$$
$$2RSH + Q \rightarrow RS-SR + QH_2\ (\Delta E_o = +0.47\ V)\ \text{Reaction 2}$$

Combining half-reactions predicts which oxidations and reductions prevail and, from the $\Delta E'_o$s, provides a measure of how energetically favourable the reactions are, that is $\Delta G_o = -nF\Delta E'_o$, in which ΔG is the Gibbs free energy, n denotes the number of electrons exchanged and F is Faraday's constant. Formal and coupled half-reactions are assumed to be at 1 M and equimolar concentrations, but they require adjustment for specific conditions. For example, mussel adhesive proteins are secreted under strongly reducing conditions with little to no oxidized Dopa or Cys-SH present. Given this, the Nernst equation[33]

$$\Delta E = \Delta E'_o - \frac{2.3RT}{nF}\log\frac{[RSSR]}{[R(SH)_2]}\frac{[QH_2]}{[Q]}$$

can approximate any ΔE relative to known $\Delta E'_o$ for inputted QH_2/Q and RSH/RSSR ratios, assuming that the R in RSH and RSSR denotes the same protein. Additionally, a pH of 7 in the above reactions is likely relevant for many biological situations; however, a correction for actual pH is necessary, as redox half-reactions involving H^+ participants are pH-dependent by definition. The secretion of byssal adhesive proteins in *M. californianus* at pH 2 (ref. 48) requires a pH adjustment for $Q + 2e^- + 2H^+ \rightarrow QH_2$ (ref. 38), in which $E'_{pH\,2}$ is +0.545 V. This is twice as resistant to oxidation than at pH 7, whereas at seawater pH 8.2, Dopa $E'_{pH\,8.2}$ is reduced to +0.18 V, which is a lower value than at pH 7.

Measuring catechol redox

Several methods have been used to detect or quantify catechol redox in mussel byssus. The easiest of these methods is via the redox reporter 2,2-diphenyl-1-picrylhydrazyl free radical (DPPH•), which has a redox potential E'_o value between that of O_2–H_2O and Dopa (Table 1) and is well-suited to reporting stoichiometric oxidation of Dopa (Reaction 3) and thiols:

$$Q + 2e^- + 2H^+ \rightarrow QH_2\ (E_o = +0.25V)\ \text{Half-reaction a}$$
$$2DPPH^\bullet + 2e^- + 2H^+ \rightarrow 2DPPH-H\ (E_o = +0.54\ V)\ \text{Half-reaction d}$$
$$2DPPH^\bullet + QH_2 \rightarrow 2DPPH-H + Q\ (\Delta E_o = +0.29\ V)\ \text{Reaction 3}$$

Oxidized DPPH• has an intensely purple colour (λ_{max} = 517 nm) that becomes pale yellow through reduction to DPPH-H[49] (Fig. 2a). DPPH•-imbibed membranes presented to plaques decolourize directly beneath each plaque[50]. Cyclic voltammetry (CV) is ideal for detecting catechols in solution or films. The CV probe contains working, counter and reference electrodes, and it involves measuring a current over a scanned range of potentials. For investigating plaque interfaces, the working electrode was a gold film onto which mussels readily attach[51] (Fig. 2b). For more analytical insights about plaque protein biochemistry, fresh plaques were mounted by double-stick tape onto sample plates, treated with a matrix such as sinapinic acid and irradiated with a pulsed ultraviolet laser light during matrix-assisted laser desorption/ionization (MALDI) time-of-flight mass spectrometry experiments[52] (Fig. 2c). Desorbed and ionized proteins with Dopa can be readily identified by 16 Da Δm increments associated with hydroxylation and searched for in mussel foot protein (Mfp) databases[53]. Because ultraviolet laser irradiation of plaques has a 1–2 µm penetration depth, another method involving horizontal electrophoretic transfer (blotting) of plaque proteins to a membrane followed by MALDI mass spectrometry of transfer spots was developed to confine the search to interfacial proteins (Fig. 2d). Accordingly, only soluble interfacial proteins were detected. Because of the prominence of Dopa in mussel adhesive proteins, for example, ten out of 50 residues consist of Dopa in Mfp3, Dopa oxidation damage can easily be tracked by time-dependent changes in mass during MALDI analysis: with a mass loss of 2 Da per each Dopa oxidized to Q, Mfp3 mass decreases by as much as 20 Da[52].

Mussel byssus

In the sections below, we describe three distinct redox microenvironments or niches in byssal threads: in the plaque, in the cuticle and in the thread core. Thiols appear to provide crucial reducing electrons to counteract Dopa oxidation in the plaque and cuticle, but this view is challenged by the ease of thiol oxidation. Protein-phase behaviour is key to insulating byssal thiols and Dopa from oxidation and provides the basis for the intrinsic repair of oxidation damage.

Thread tenacity and redox

In adult *M. californianus*, byssal threads are 2–8 cm long (with a diameter of ≤1 mm), ending distally in flared plaques with diameters of 2–5 mm (Fig. 1a). Distal thread tenacity resembles high-end Nylon-6 filaments[54,55], the mechanical details of which[17,55] are not at issue here. One property worth noting, however, is thread self-healing — despite an apparent yield at ~0.2 strain during uniaxial tension, the thread core and cuticle exhibit nearly complete, time-dependent recovery of the initial modulus, strength and length[55,56]. Such behaviour involves energy dissipation, adding tremendous shock-absorbing capabilities to the byssus and hints at the presence of reversible sacrificial bonds. That catecholato-metal ion complexes directly define initial modulus and hardness in byssal cuticle was elegantly shown by nanoindentation of pristine, ethylenediaminetetraacetic acid (EDTA)-depleted and Fe^{3+}, V^{3+} and Al^{3+}-reconstituted threads[28]. Not only did metal ion depletion reduce stiffness by ~85%, but iron restoration returned it to pristine levels.

Q–QH_2 electrochemistry clarifies the context-dependent question of whether Q or QH_2 will prevail, but how does QH_2 redox relate to architecture and mechanical deformation? A 'redox niche' model of mussel byssus proposed that three different Q–QH_2 microenvironments[57,58] — namely, thread cuticle, core and a plaque adhesive interface — coexist within each byssal thread. Each niche or microenvironment has a distinct redox tendency. QH_2 is favoured in the plaque and cuticle, whereas Q prevails in the thread core. Additional niches may exist.

Plaque redox niche

The junction between a byssal plaque and a solid substratum is essentially a coating adapted for adhesion to a solid surface (Fig. 1b). The architecture of this region is quite distinctive. The interface itself is a thin, uniform (<10 nm), wrinkled skin or film (Fig. 3a,b). Above the film is an intricate open-cell porous scaffold with two length-scales of porosity, averaging 50 nm-diameter and 1–2 µm-diameter pores,

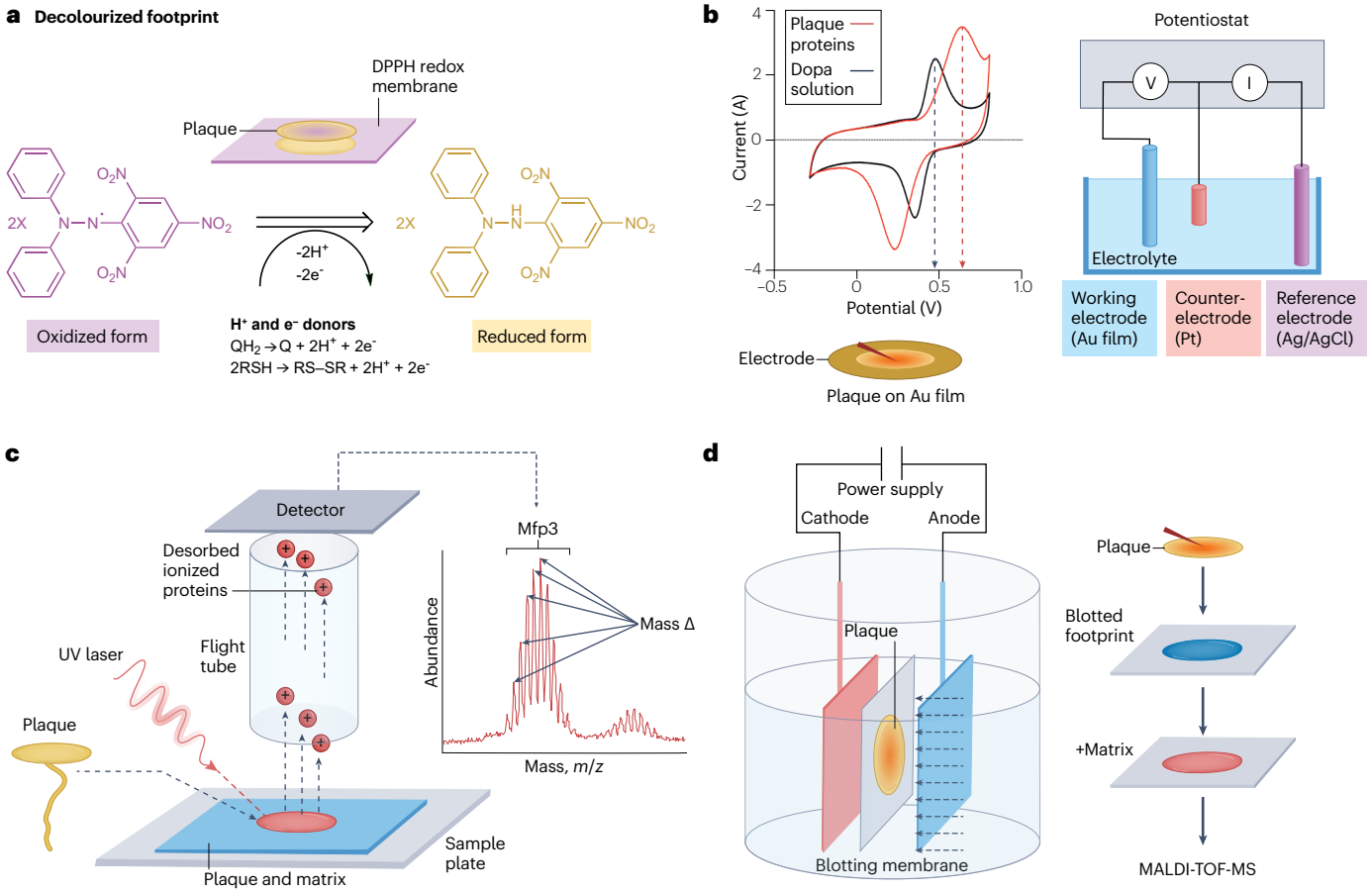

Fig. 2 | Measuring catechol redox in mussels. a, 2,2-Diphenyl-1-picrylhydrazyl free radical (DPPH$^{\bullet}$) is a redox reporter that visibly changes colour from purple in the oxidized form to pale yellow in the reduced form. Reporting by DPPH$^{\bullet}$ can be conducted in solution or in the solid state, as in membrane footprint testing, in which the reducing plaque underside decolourizes a corresponding spot on the DPPH redox membrane[50]. **b**, Cyclic voltammetry combines three electrodes (working, counter and reference) to measure catechol redox activity in solution or at an interface. The set-up shown detected catechols at an intact plaque/gold film interface[51]. **c**, Plaque interfaces are also accessible to interrogation by in situ matrix-assisted laser desorption/ionization time-of-flight mass spectrometry (MALDI-TOF-MS). In this case, plaques are secured upside-down by double-stick tape with the plaque underside coated by a matrix such as sinapinic acid, in order to detect desorbed and ionized proteins[52]. **d**, Given the 1–3 µm-deep penetration afforded by UV lasers, horizontal electroblotting followed by MALDI-TOF-MS analysis enables more selective transfer of interfacial proteins[51]. Both MALDI-TOF-MS methods can detect protein hydroxylation by Δ16 Da ladders and oxidation by cumulative 2 Da losses. Dopa, 3,4-dihydroxyphenyl-L-alanine; UV, ultraviolet.

respectively, dispersed within a spongy trabecular mesh[59]. The pores are naturally fluid-filled but usually drain during fixation and sectioning for microscopy, so they appear empty; however, freeze-fracturing plaques appears to preserve the fluid filling[60].

The distalmost 3 µm of each plaque is dominated by four proteins: Mfp2, Mfp3, Mfp5 and Mfp6 (Fig. 3b). The trabecular mesh of Mfp2 surrounds an interconnected system of fluid-filled pores. Mfp2 was shown by resonance Raman microscopy and the surface forces apparatus (SFA) to undergo reversible cross-linking via Fe^{3+}-Dopa complexes, thereby endowing it with a cohesion energy of −2.2 mJ m^{-2} in the pH 5.5–6.8 range[61,62]. A useful metric for comparison is the energy to separate biotin-functionalized from streptavidin-functionalized surfaces in the SFA: at about −10 mJ m^{-2} (pH 7), this energy represents a protein–ligand interaction that is noncovalent but nearly as strong as a covalent bond[63]. As amplified in the next section, bidentate catechol-metal ion complexes approach the bond energy of a covalent bond, yet they are completely reversible[14]. Besides its ~5 mol% Dopa content for Fe^{3+} complexation, Mfp2 (45 kDa) consists of 11 tandem epidermal growth factor (EGF) repeats and 33 intramolecular disulfide bonds (7 mol%)[61] (Fig. 3c).

Mfp3 and Mfp6 co-reside in droplets within the plaque pores[51]. Mfp3 is a heterogeneous family of >30 variants with low mass, 5–7 kDa[64] (Fig. 3b,c). In variant Mfp3f, for example, Gly is the dominant amino acid (24%), followed by Dopa and Arg/4-hydroxyarginine (both 20 mol%). The high density of polar and charged residues supports an intrinsically disordered protein structure[65]. Mfp6 comprises five–six similar variants, which are characterized by a mass of ~11.6 kDa and an isoelectric point (*pI*) between 10 and 11. The high density of polar and charged residues again favours an intrinsically disordered protein, although 2D NMR data suggest a small β-sheet core[47]. Thiol cysteine is abundant at 9–10 mol%, but Dopa is also present at 4–5 mol%. Mfp5 (9 kDa; *pI* ~8–9) is detectable in small amounts between the plaque and substratum, and

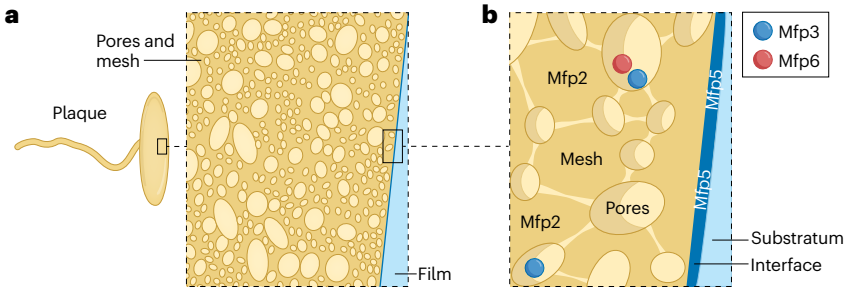

c

Sub-niche	Mfp protein	Mass (kDa)	QH_2 mol%	RSH mol%	-SS- mol%	Tension (40% strain)	Redox ratio oxidized/reduced (local concentration)	Redox tendency
Pore droplets	Mfp3 Mfp6	5–7 12	20 5	0 11	0 0	Fluid	Q/QH_2: 1/20 (0.7M); -SS-/RSH: 1/11 (0.4M); medium O_2 (250 uM)	Reducing → QH_2
Mesh scaffold	Mfp2	45	5	0	7	No	$[Fe^{3+}(Q^{2-})_3]^{3-}$/QH_2: ~5/<1 -SS-/RSH: ~7/<1 medium O_2 (250 µM)	QH_2-protected slightly oxidizing
						Yes	-SS-/RSH: ~7/<1; Q/QH_2: ~1/5 medium O_2 (250 µM)	Oxidizing → Q
Interface	Mfp5	9	26	0	0	No	Metal oxide = (Q^{2-})/QH_2: ~25/<1 medium O_2 (250 µM)	QH_2-protected slightly oxidizing
						Yes	Q/QH_2: ~1/26 medium O_2 (250 µM)	Oxidizing→ Q

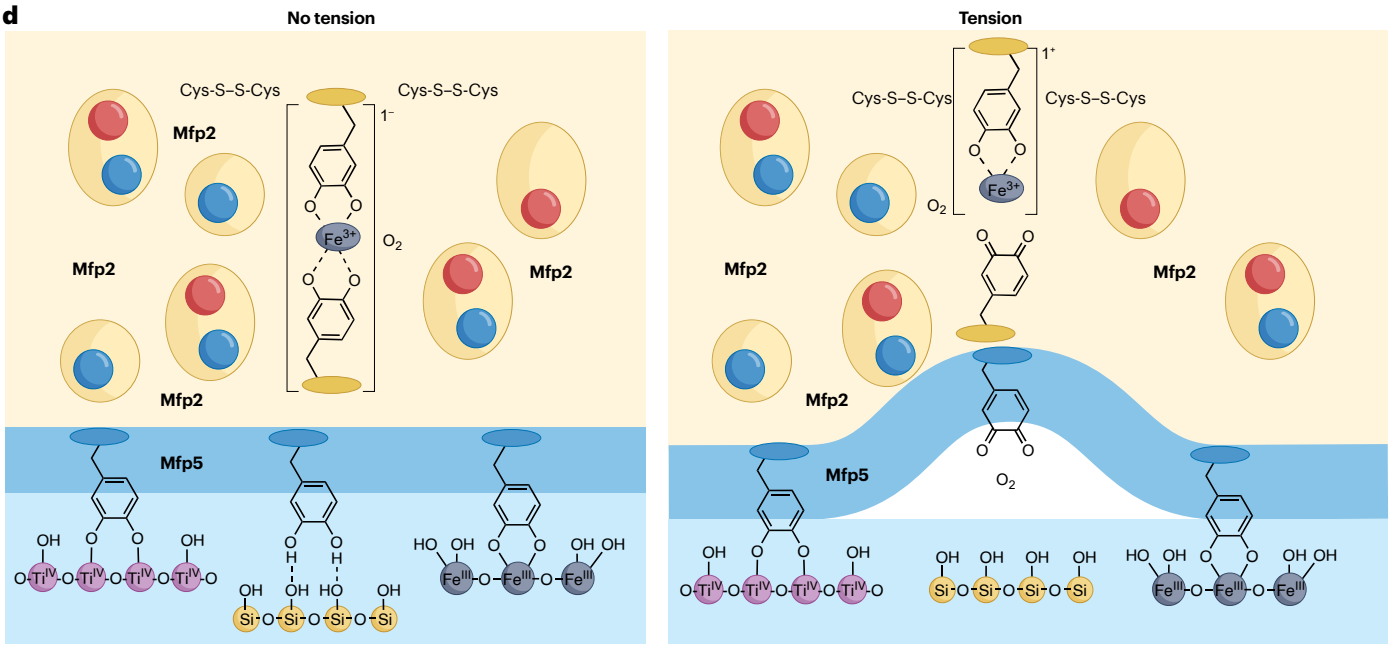

Fig. 3 | Catechol redox in byssal plaques. a, Drawing of a byssal plaque section enlarged near the plaque–substratum interface; it consists of a continuous priming film, a trabecular scaffold and fluid-filled pores with two distinct length scales: 1 µm and 50–100 nm. **b**, An illustration of magnified pores shows the distribution of major proteins – Mfp2, Mfp3 and Mfp6, and Mfp5 and fine droplet interconnections. **c**, A tally of major plaque proteins, their content of redox-active Dopa (QH_2), cysteine (RSH) and cystine (-SS-), and redox tendencies in the absence (No) or presence (Yes) of applied tension (40% strain)[75]. Q^{2-} denotes catecholate, and local concentrations were estimated using the wt% protein in coacervates and known Dopa/cysteine contents[51]. **d**, Correlation of catechol coordination with plaque microstructure and how mechanical deformation changes chemical interactions and redox vulnerability. When slack (no tension), Dopa reactivity is passivated by stable metal ion and surface oxide complexes. Surface oxide complexes bidentate binuclear (Ti^{IV}) and (Fe^{III}) are based on catechol interactions with anatase[124]. During tension, surface delaminations and internal tears lead to Dopa exposure and oxidation. Drawn from micrographs in refs. 74,75. Dopa, 3,4-dihydroxyphenyl-L-alanine; Q, *o*-dopaquinone.

it requires nearly double the laser power as any other Mfp to desorb from surfaces by MALDI time-of-flight mass spectrometry. Consistent with its surface-priming function, Mfp5 distribution is confined to the interface and has a composition dominated by Dopa and Lys (both ~25 mol%) that work synergistically in adhesion to mica[52,66,67] (Fig. 3b,c).

With so much Dopa at the interface, spontaneous conversion to Q would be expected at seawater pH (~8) and E'_o of +0.86 V[68], but this is not the case. Indeed, studies indicate that plaques remain indefinitely reducing. For example: 1) plaque interfaces reduce DPPH$^{\bullet}$ (E'_o +0.3 V at 20 °C) to DPPH-H for at least 21 days post-secretion[50]; 2) plaques deposited by mussels onto gold films and subjected to CV showed considerable current at anodic potentials, corresponding to catechol oxidation, and much lower or no current at $E_{cathodic}$[51] (Fig. 2d); 3) proteins horizontally transferred from mature plaques at different ages to blotting membranes, and, when analysed by mass spectrometry, had >95% of their Dopa intact[51]; finally, 4), although both Dopa and Cys have the ability to reduce DPPH$^{\bullet}$, in Mfp6, DPPH$^{\bullet}$ reduction by Cys was tenfold faster than reduction by Dopa[47].

The interdependence of redox and adhesion was resolved by SFA measurements of the adhesion of various purified plaque proteins to mica. Freshly cleaved muscovite mica has an atomically smooth aluminosilicate surface with a capacity for H-bonding and perhaps alumina-silica chelation[69]. Mfp3 and Mfp5 exhibited the best adhesion at pH 2–3 with a span of SFA adhesion energies between −2 and −15 mJ m^{-2} for Mfp3 and Mfp5, respectively[70,71]. Adhesion energy was inversely correlated with pH, decreasing to <−1 mJ m^{-2} at pH 7 (refs. 70,71). Although adhesion losses were irreversible with respect to pH, adhesion was restored by adding nanomolar amounts of Mfp6 to the interface. Recalling that Mfp6 contains both thiol and catecholic groups, a thiol-coupled redox recovery was demonstrated by S-carboxymethylation of Mfp6, which abolished ~80% of adhesion recovery on mica. Collectively, the data support the inference that Dopa residues in purified Mfps are vulnerable to spontaneous oxidation in solution at pH 7–8, which in turn contributes to adhesion loss, because it is the catechol not the quinone that interacts effectively with mineral and metaloxide surfaces[14,72]. It was not possible to present stable catechols to mica for adhesion at pH 8 in the SFA, but monocatecholato-boronate complexes protect catechols from oxidation to quinones long enough at pH 8 to allow catechols to exchange borate for competitive binding to surface groups. In the short term, Mfp5 showed comparable adhesion at both pH 3 and 8 in borate buffer[73].

Although reducing overall, the byssal plaque contains at least three sub-niches: mesh, pores and interface (Fig. 3c). In unstressed plaques, the mesh and interface are moderately oxidizing, but there is little to oxidize, as most Dopa is passivated by stable chelation to Fe^{3+} or chemisorption to surface metal oxides, and Cys (in Mfp2) is entirely disulfide-bonded. By contrast, pore droplets are strongly reducing[51]. Tensile deformation of plaques revealed that the adhesive fracture energy of whole-plaques was 6,500-fold greater than the SFA-based adhesion energy for Mfp5 over the same surface area, suggesting substantial dissipative restructuring in plaques visible as reversible plaque elongation in the mesh and partial delamination at the interface[74] (Fig. 3d). Higher availability of Fe^{3+} in ambient seawater greatly improved plaque cohesion[60]. Ruptured catecholato-Fe^{3+} or catecholato-oxide complexes expose Dopa, making it easy prey to oxidation[8]. Nothing is known about how tensile deformation of plaques affects pore droplet contents but, with open pores, content mixing seems likely. Nernst equation calculations based on Dopa and Cys contents of Mfp3 and Mfp6 (refs. 38,51) (~0.4–0.7 M) predict a droplet $\Delta E'_o$ of about +0.55 V (pH 8), which is easily sufficient to drive external Q back to QH_2, assuming facile H^+ and e^- transfer between sub-niches.

Cuticle redox niche

The byssal cuticle faces ambient seawater. Microscopic examination of sectioned byssal threads reveals an anisotropic fibrous core covered by an outer layer ~2–5 µm-thick with a distinctly composite structure: discontinuous spherical granules or particles (1 µm in diameter) dispersed in a continuous matrix (Fig. 4a). Indentation analysis of hydrated threads revealed that the cuticle is ~sixfold stiffer and harder than the core[75] and that the spherical granular inclusions are more hydrated and a third as stiff as the surrounding matrix[76]. A transmission electron microscopy image of sectioned particles exhibits a convoluted and folded internal organization at high magnification (Fig. 4b). Resonance Raman detected a high density of catecholato-Fe^{3+} coordination complexes in cuticles[27,28]. Accordingly, bis-catecholato-Fe^{3+} and tris-catecholato-Fe^{3+} complexes are present throughout the cuticle but at ~fivefold higher concentrations in the granules than the continuous matrix (Fig. 4c). The only known cuticular Dopa-containing protein is Mfp1, which in *Mytilus* species consists of 65–75 tandemly repeated decapeptides with 1–2 Dopa residues per decapeptide that bind Fe^{3+} in both bis and tris modes at pH 5–8 with a cohesion energy of −4.5 mJ m^{-2} in the SFA[77,78] (Fig. 4c). Soluble Mfp1 is susceptible to Lys-C-endopeptidase and trypsin digestion[77], but not after Fe^{3+} complexation. The high-affinity metal coordination exhibited by catechols including Dopa is attributed to a ligand-to-metal $\pi \rightarrow d$ orbital transition and charge-transfer[79,80]. The tris-catecholato-Fe^{3+} stability constant of Mfp1 exceeds log K_s = 40 (ref. 81), which is not surprising, given that mussels must compete with microbial catecholic enterobactins for the limited supply of soluble Fe^{3+} in seawater[30]. By comparison, Fe^{3+}-EDTA has a log K_s of only 25 under similar conditions[81].

Cuticles of threads pulled to 30–40% strain and inspected by scanning and transmission electron microscopy exhibited, at first, granule elongation, followed by the formation of a fine network of nanotears in the continuous matrix averaging ~50 nm in width[75] (Fig. 4b). At >100% strain, the nanotears merged into microtears with lower reversibility and ~2–5 µm gaps that were large enough to accommodate *Vibrio* and other marine bacteria that degrade the core with aggressive collagenases[82,83]. Because the nanotears are reversible, much effort went into testing, replicating and modelling the tear chemistry as reversible mechanochemical complexes — namely, octahedral hexadentate bis-catecholato-Fe^{3+} and tris-catecholato-Fe^{3+} chelates[79,81]. Accordingly, the less dense matrix tris complexes are readily torn asunder during extension, creating[8,22], for example, first one and then two free catechol ligands, and a monocatecholato-Fe^{3+} complex, as confirmed by dynamic molecular modelling[84] (Fig. 4c). Coupled redox Half-reactions a + b predict that catechols not protected by the stability of tris complexes become susceptible to oxidation at seawater pH. Dopa-containing proteins like Mfp1 are not limited to forming Fe^{3+} complexes, but include V^{3+} and Al^{3+} in tris-catecholato complexes[28], the former resulting in cohesion superior to Fe^{3+} (ref. 85). In addition, a binding half-life is associated with an average 'on' time for catechols in sheared tris-catecholato-metal ion complexes in polymeric hydrogels. For example, Al^{3+}, Fe^{3+} and In^{3+} all formed tris complexes of comparable stability with catechols, yet rheological analysis showed half-life values of 100, 23 and 2.8 s,

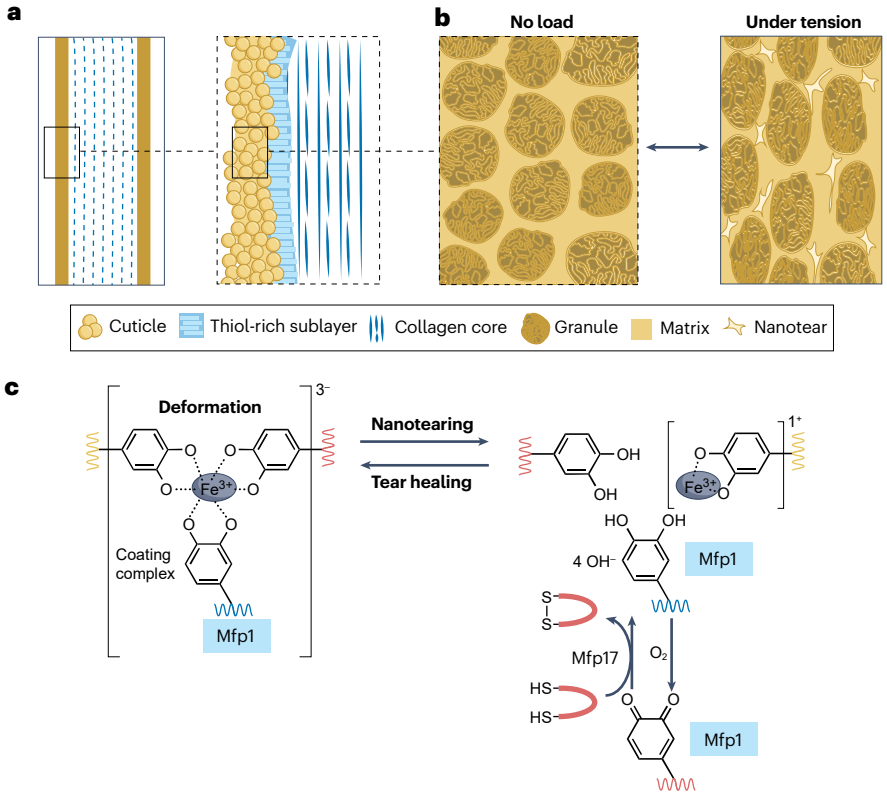

Fig. 4 | Catechol redox in the byssal cuticle. **a**, Thread (diameter: 0.15 mm) section shows an anisotropic core of mostly collagen coated by a granular cuticle. Thread treatment with thiol-specific fluorescent probes highlights a cuticular sublayer (light blue) in which thiols are concentrated[87]. **b**, Granules are roughly spherical, 1–2 µm in diameter, with convoluted interiors. As a result of cuticle tension, the granules elongate reversibly, a process followed by reversible microtearing in the matrix[27,75]. **c**, A scheme showing the mechanochemistry during uniaxial tension as well as the change in susceptibility to oxidation. Thiol-rich proteins restore 3,4-dihydroxyphenyl-L-alanine (Dopa) exposed to oxidation during catecholato–Fe^{3+} bond rupture. **d**, A tally of major cuticle proteins, their redox-active Dopa (QH_2) and cysteine (RSH) contents, and redox trends in the absence (No) or presence (Yes) of applied tension. Q^{2-} denotes catecholate, and local concentrations were estimated using the hydrated volume of each protein. When Dopa content is unknown, Tyr levels are denoted. Other than Mfp1 and Mfp17, all proteins are putative based on mussel transcriptomes[53]. Q, *o*-dopaquinone.

d

Sub-niche	Mfp protein	Mass (kDa)	QH_2 mol%	RSH mol%	Tension (40% strain)	Redox ratio oxidized/reduced	Redox tendency
Cuticle	Mfp1	110	15	0	No	$[Fe^{3+}(Q^{2-})_3]^{3-}/QH_2$: ~15/1 medium O_2 (250 µM)	QH_2-protected
					Yes	Q/QH_2: ~1/15 medium O_2 (250 µM)	Oxidizing → Q
Sublayer	Mfp16 putative	10.6	(3Tyr)	17		Unknown	Unknown
	Mfp17	23.6	(8Tyr)	7	Fluid	RSSR/RSH: ~1/7 medium O_2 (250 µM)	Reducing → RSH
	Mfp18 putative	7.9	(12Tyr)	19		Unknown	Unknown

respectively[86]. In other words, the probability of catechol oxidation in these tris-catecholato-metal complexes follows the trend In^{3+}>Fe^{3+}>Al^{3+}. Quinones are inferior donor ligands for Fe^{3+} (ref. 79), so the reformed tris complexes are weakened[14,72], leading to poorer abrasion resistance, larger microtears and greater microbial penetration during subsequent wave cycles. As thread cuticles in the field are quite durable, strategies resembling those at the plaque interface to counteract oxidation damage merit investigation.

The transcriptome of *M. californianus* byssus revealed that several Cys-rich proteins are expressed by the cuticle-forming gland[53], but their distribution and function in the cuticle were unknown. Using a thiol-specific fluorophore and confocal microscopy, Valois et al.[87] detected a soft thiol-rich sublayer 3–5 µm-thick between the cuticle and core (Fig. 4a). Presumably by dint of its Cys thiol content, each thread released 1.5 times more e^- and H^+ equivalents to the redox reporter $DPPH^•$ than the spontaneous exchange between 0.1 µmole Cys and $DPPH^•$ in solution. Mfp17 was partially characterized, but it is not the only Cys-rich (15 mol%) cuticle protein – three others with high Cys and intrinsically disordered protein structures have been predicted[53] (Fig. 4d).

Recalling that mechanically ruptured tris-catecholato-Fe^{3+} complexes mediate reversible microtearing and that Dopa ligands wrested from Fe^{3+} are prone to undergo oxidation to quinones, Reaction 2 predicts that quinones will be restored to Dopa by e^- and H^+ from Mfp17 and other thiol-rich proteins in the interlayer (Fig. 4c). Still missing are details regarding how the reducing equivalents in the sublayer are insulated from seawater oxygen and shuttled from the sublayer to cuticle-damage points. H^+ and e^- shuttling between thiols and quinones is common in the periplasmic space of bacteria[88]. Bacteria are equipped with a cascade of thiol-rich proteins (thioredoxins) to perform redox shuttling and form an obligatory charge-transfer complex between thiolate, Arg and quinone before reducing the quinone[89]. Arg involvement in periplasmic charge transfer is intriguing, given the Arg-rich composition of Mfp3 and Mfp16 variants[53,64].

Core redox niche

Some Dopa oxidation is necessary for the maturation of byssus. Byssal threads made under hypoxic conditions are weaker in cohesion than those made at normoxia[90]. The oxidizing thread core represents >90% of the thread volume and contains a cross-linked anisotropic assembly of protein microfibres derived from smectic mesophases secreted by the foot[91]. The mesogenic precursor collagens in mussel byssus known as preCOL-D (Fig. 5a) and preCOL-P[92] are molecular chimaeras of trimeric collagen with silk-fibroin or elastin flanking domains, respectively, and are swathed by a small amount (<2% dry weight) of thread matrix protein (TMP)[93]. The C-termini and N-termini of each preCOL trimer have clusters of 6–12 Dopa residues (~0.4 mol%)[92] – TMP swathing adds as many as ~26 Dopa residues per protein[93]. At seawater pH 8.2, an E'_o of +0.8 V and no reservoir of reducing H^+ and e^- conditions are very favourable for *o*-dopaquinone formation (likely to be enzyme-catalysed) leading to cross-linking. The mussel foot transcriptome contains at least a couple of tyrosinase-like sequences, but these have yet to be investigated as catalysts in byssus[53].

In the mesophase formed by preCOLs, *o*-dopaquinones destined for cross-links in preCOL-D are in close proximity to several potential nucleophilic partners, namely, Lys and His residues for Michael-type or Schiff-base-type cross-linking[36,58]. C-terminal His occurs thrice per chain and is precisely aligned with Dopa in an antiparallel sequence coming from the neighbouring preCOL in the train (Fig. 5b) – similarly, N-terminal Dopa lines up with Lys. As a rule, nucleophiles must be deprotonated prior to forming Michael or Schiff-base adducts with quinones. Solvent-accessible pK_a values for Lys and His are 10.4 and 6.4, respectively. Catechol–His cross-links, such as those in insect cuticles[94] and squid beaks[95], are likely due to the co-abundance of Dopa and His in any pair of coupled C-terminal preCOL-D sequences (Fig. 5c), whereas Lys–Dopa adducts have been detected in coupled N-termini of adjacent preCOLs[58]. High-yield cross-link formation in macromolecules between Q and its nucleophile partners requires proximity[96] – a condition that is satisfied by orderly head-to-head, tail-to-tail preCOL arrays. The Dopa-derived cross-links are functionally important to cohesion, because they are the only known covalent bonds securing each train of successive preCOLs in the core-based microfibres[41] that extend deep into the plaque.

Although Dopa-derived cross-links define irreversible end-to-end connections between preCOLs, there are also His-Zn complexes in preCOL-D that are associated with flanking $[His\text{-}Ala]_9$ repeat sequences[97] (Fig. 5a). Upon secretion and deprotonization at pH 8, 3–4 His residues per chain are recruited for complexation to each Zn^{2+} and, during cyclic loading, one or more His ligands break reversibly from Zn upon extension to dissipate energy[97]. In a fascinating counterpoint to the strong non-innocent[98,99] tris-catecholato-Fe^{3+} complexes of the cuticle, the somewhat weaker His-Zn^{3+} complexes in the core involve stable, innocent ligands and metal nuclei[90] as appropriate for this oxidizing niche.

Conundrum regarding thiol redox. The redox poise provided by thiol-rich proteins in reducing niches is necessary to maintain the adhesion of Dopa-containing proteins, particularly if the latter engage in metal-ion coordination and/or interfacial H-bonding interactions[64]. The redox potentials of the disulfide–thiol and quinone–catechol half-reactions make this highly plausible, but it also reveals an unsettling conundrum. Combining the half-reaction for thiols (2R-SH to R-S–S-R) with O_2 reduction (Reaction 4) results in a $\Delta E'_o$ that is twice as favourable as the oxidation of Dopa to *o*-dopaquinone.

$$2RSH \rightarrow RS-SR + 2e^- + 2H^+ \ (E_o = \sim -0.22\ V)\ \text{Half-reaction c}$$
$$1/2O_2 + 2e^- + 2H^+ \rightarrow H_2O \ (E_o = \sim +0.82\ V)\ \text{Half-reaction b}$$
$$1/2O_2 + 2RSH \rightarrow RS-SR + H_2O \ (\Delta E_o = +1.04\ V)\ \text{Reaction 4}$$

In other words, Dopa restoration that is reliant on reductive rescue by thiols is a nonstarter if both Dopa and thiol are accessible to O_2. Indeed, exposure of Mfp6 to DPPH$^\bullet$ is an apt reminder of this because nine thiols in Mfp6 were oxidized before the slower Dopa oxidation occurred[47]. These results support the proposition that, if H^+ and e^- are provided as needed from thiols and Dopas to maintain a reducing poise, they must be stowed in reservoirs that are somehow insulated against oxidation. It is appropriate to ask if such reservoirs exist. In an extracellular matrix such as tendon, redox poise is maintained

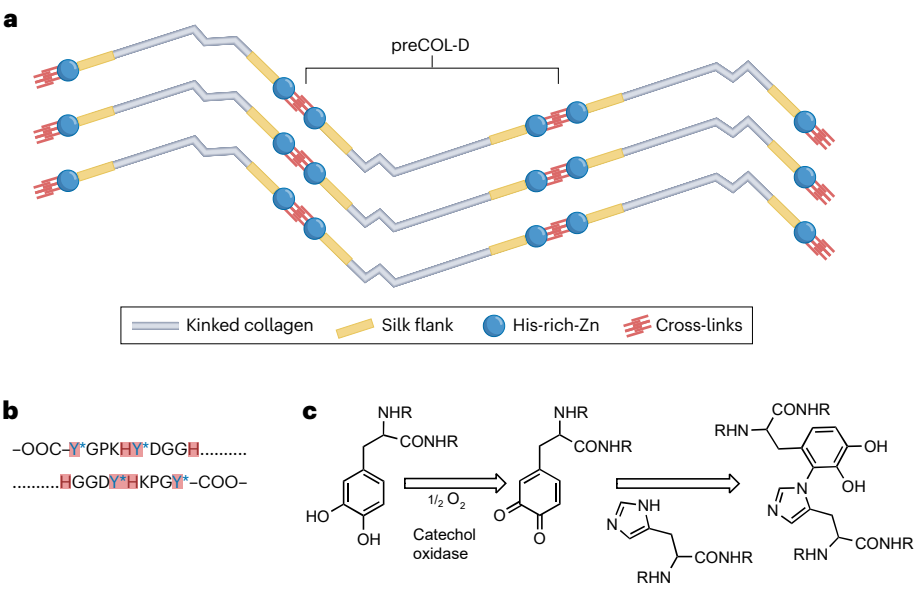

Fig. 5 | Catechol redox in byssal core. a, A self-assembled core collagen known as preCOL-D (*Mytilus edulis*) with its flanking His-rich and silk domains. **b**, A zoom of paired C-terminal cross-linking sequences from two different consecutive preCOL-Ds is enlarged, showing alignment of C-terminal Lys (K), His (H) and Dopa (Y*) residues[91]. **c**, After Dopa is oxidized to the corresponding quinone, deprotonated His and Lys (pH 8) residues undergo Michael/Schiff-base additions with quinone neighbours. A 5-*N*-histidyl-Dopa cross-link is shown[94,95]. *Mytilus* byssus contains catecholoxidase[125], but not tyrosinase, activity. Dopa, 3,4-dihydroxyphenyl-L-alanine.

by embedded fibroblasts via the costly production and secretion of reduced glutathione[99]. This is not an option in acellular mussel byssus.

Phase separation and redox. One mechanism for insulating reducing reservoirs involves coacervation, in which water-soluble biomolecules, often polyampholytes, become water-insoluble as dense polymer-rich droplets[100]. Coacervation of polycations and polyanions is often initiated by extensive Coulombic interactions. However, the greater part of ΔG comes from the increased entropy associated with the release of micro-ions and water from the polymer-dense phase[101,102].

Involvement of Mfp coacervation in byssus was first suggested from observations that an Mfp3 variant extracted from byssal plaques coacervated reversibly by adjustments to pH and ionic strength[103]. Additional recombinant[103,104] and purified Mfp proteins[105] were shown to coacervate by different modes: intrinsically[106], by adding multivalent anions (such as phosphate, citrate and sulfate)[46,104,106,107] and by high ionic strength[108]. Coacervation by the high-ionic-strength mode demonstrated that polycations could phase-separate without a polyanionic partner when aromatic molecules were present. Coacervation triggered by cation–π interactions[108] is a fascinating case in point: Mfp1 with ~20 mol% Lys and Dopa/Tyr coacervates poorly at ~0.1 M salt, because it comprises both attractive R-NH_3^+–π and repulsive R-NH_3^+–R-NH_3^+ interactions, However, at seawater salinity (0.7 M) cation–cation repulsions are more effectively screened than R-NH_3^+–π interactions, and coacervation is thus enabled. This trigger is also relevant to other high-*pI* Mfps having cation-aromatic-rich compositions.

With respect to redox reservoirs, Dopa and thiols in coacervated droplets of Mfp3 and Mfp6 were >tenfold more resistant to oxidation than those in solution[51]. When followed by confocal microscopy using intrinsic or thiol-tagged protein fluorescence, plaque-derived Mfp3 and Mfp6 exhibited a rapid growth of the dense coacervated phase following addition of sulfate, undergoing independent phase separations before coalescing as heterogeneous droplets. Within the first 60 min of exposure to oxidants, these droplets resisted redox exchange with 0.1 mM DPPH$^{\bullet}$ and 10 mM periodate, contrary to the parallel solution controls. Resistance is unlikely due to lower oxidant solubility in the dense phase.

The existence of two redox-active agents — thiol and catechol — within the same droplets (Fig. 6a) is intriguing because it begs the question as to whether thiol, catechol or both, shuttle H^+/e^- to the external environment. We favour the catechol for this for four reasons: 1) if repair is primarily for Q reduction, then the catechol would enhance the specificity of quinone binding by its bidentate H-bonding to Q[109]; 2) catechols lower the risk of energy loss as the $\Delta E'_o$ of two coupled Q/QH_2 half-reactions is less (Reaction 5), for example

$$Q_A + 2e^- + 2H^+ \rightarrow Q_AH_2 \ (E'_o = \sim +0.25\ V)$$
$$Q_BH_2 \rightarrow Q_B + 2e^- + 2H^+ \ (E'_o = \sim -0.21\ V)$$
$$Q_A + Q_BH_2 \rightarrow Q_AH_2 + Q_B \ (\Delta E'_o = +0.04\ V) \quad \text{Reaction 5}$$

(here Q_AH_2 and Q_BH_2 denote distinct Mfp Dopas with different redox potentials); 3) thiol exchange with the external environment might undermine the structural integrity of the Mfp2 mesh by reducing some or all of its critical 33 disulfides; and 4) Dopa is restorable from the quinone, but there is no redox exchange within droplets that is capable of restoring thiols. In the model (Fig. 6a), when oxidative service damage occurs in either cohesion or adhesion, droplet Dopa provides $2H^+$ and $2e^-$ for external Q reduction, thereby restoring adhesion or cohesion. Droplet Q then either undergoes redox exchange with two thiols to restore droplet Dopa or tautomerizes to form dehydroDopa (a vinyl-catechol) for another redox exchange cycle with external Q. Both modes have been observed[110].

To get at the mechanism of oxidative resistance within coacervates, Valois et al.[51] turned to CV using the catecholic moiety of Dopa in Mfp3 as an intrinsic redox reporter. The anodic potential of peak current for Mfp3 Dopa increased by ~200 mV when in a coacervated state with respect to the solution state. Given the slow electron exchange of thiols with solid electrode surfaces, tracking thiol redox by CV was not feasible in these experiments. To further explore phase-dependent redox, coacervates were made with a variety of synthetic and commercial polyelectrolytes and combined with 4-methylcatechol[111]. Poly-*L*-Lys/poly-racemic *D, L*-Glu coacervates, for example, accumulated 4-methylcatechol to 15-fold the equilibrium solution concentration, whereas poly(2-(dimethylamino)ethyl-methacrylate) and gum-arabic concentrated 4-methylcatechol to 250-fold. Notably, once inside the coacervate, 4-methylcatechol showed a ~250 mV enhancement in anodic potential as well as a much-improved resistance to periodate oxidation[111]. Natural-abundance ^{13}C aromatic heteronuclear multiple quantum correlation NMR of coacervates detected considerable self–self bidentate H-bonding between two to three 4-methylcatechols (Fig. 6b) previously only detected in crystals,

Glossary

Byssus
A holdfast made of specialized extra-organismic biomacromolecules and produced by the foot in bivalve molluscs, especially mytilid mussels.

Coacervation
A desolvation of water-soluble molecules leading to the formation of two phases: a dense protein-rich or polymer-rich phase and a dilute solute-depleted equilibrium phase. Often referred to as liquid–liquid phase separation.

Homeostasis
In redox systems, an energy-dependent tendency towards maintaining a relatively stable equilibrium between oxidized and reduced analytes.

***Mytilus* species**
A large genus of byssally-attached marine mussels notable for tenacity and high intertidal distribution throughout the world. Most of the biochemistry of adhesive proteins has been done on three species: *Mytilus edulis* Linnaeus, *Mytilus galloprovincialis* Lamarck and *Mytilus californianus* Conrad.

Niches
Microenvironments within functional mussel byssus (such as the cuticle, plaque or core) that exhibit a distinct redox preference for either catechol or o-quinone.

Plaques
The flared portions at the distal ends of each mussel byssal thread that are specifically adapted for underwater adhesion to solid surfaces, including other mussel shells, rocks, pilings and a variety of synthetic polymers.

Redox poise
In functioning byssus, redox poise is an adaptive redox balance in which either o-quinone or catechol is favoured. Favouring catechol in seawater requires a steady supply of e^- and H^+ to repair losses due to inevitable oxidation.

Transcriptome
A complete library of mRNA present at any particular stage of a cell and or organism. Additionally, although indirectly, a library of potentially translated proteins.

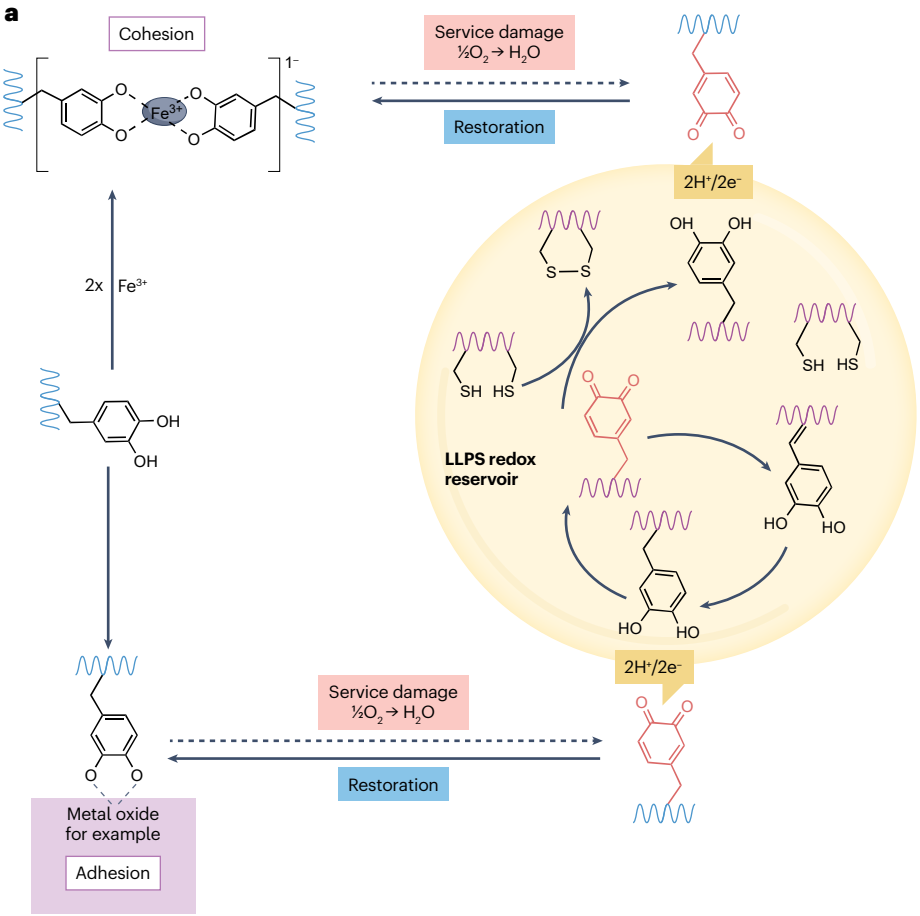

Fig. 6 | Model of liquid–liquid phase-separated coacervates as redox reservoirs and coacervate-specific interactions. a, Damage during cohesive/adhesive service occurs when 3,4-dihydroxyphenyl-L-alanine (Dopa)-metal ion or Dopa-surface oxide complexes are mechanically ruptured, and exposed Dopa gets oxidized to the corresponding *o*-quinone (red). Liquid–liquid phase-separated mussel foot proteins (yellow) are able to store and donate H^+ and e^- to *o*-quinone by insulating their redox-sensitive cargo of Dopa and cysteine from other oxidants in the ambient O_2-saturated milieu. To provide reliable redox poise, droplet Dopa and Cys must be able to release H^+ and e^- on demand to external quinones in the plaque or cuticle. In this way, byssal adhesion and cohesion are maintained until the droplet H^+/e^- supply is depleted. Note that droplet quinones can become vinyl-catechols by tautomerization, without depending on thiol reduction[47,110]. **b**, Noncovalent self–self interactions with the ability to enhance Dopa and Cys stability against oxidation. Structure of catechol–catechol bidentate H-bonding[111] (left); structure of R-SH-σ* to aromatic ring π interactions[114] (right). LLPS, liquid–liquid phase separation.

acetonitrile[112] and in a coacervated Dopa-containing adhesive protein from the green mussel *Perna viridis*[105]. As theory predicts a 100 mV anodic potential increase for each additional H-bonded phenolic OH, a ~ +200 mV stabilization for bidentate complexes is quite plausible[113]. Noncovalent interactions between thiols and aromatic rings in proteins are also known and, on the basis of crystal structures and NMR and infrared spectroscopy data, are proposed to be present between aromatic π donors and SH σ* acceptors (Fig. 6b) with interaction energies between −2 and −5 kcal mol^{-1} (ref. 114). Although such interactions have yet to be investigated in coacervated proteins, the long-term protective effect of adding 1,4-dithiothreitol to coacervates of Mfp1 and even coacervated Mfp1 containing triscatecholato-Fe^{3+} complexes is known[115]. For example, 1,4-dithiothreitol maintained Mfp1 Dopa in a reduced form under both conditions, without competing with Dopa–Fe^{3+} binding.

Conclusions and outlook

Mussels depend on catechols in the form of Dopa-containing proteins for their byssal adhesion and cohesion properties. Particularly advantageous are the catecholato–metal coordination bonds, which exhibit high stability constants (log $K_s \geq 40$) and are half as strong as covalent bonds, yet reversible, contributing to very desirable material properties, including high stiffness, extensibility and toughness, as well as self-healing. Although some of these properties have been successfully translated to synthetic platforms, the advantages of catecholato–metal ion coordination are typically short-lived, because catechol exposure following bond rupture under stressed, oxygenated and neutral-to-alkaline pH conditions leads to quinone formation, nonspecific cross-linking and material embrittlement within days.

Mussels extend catechol lifetimes by relying on an extraordinary homeostatic adaptation. Save in the core, the majority of Dopa

functionalities in each single-use byssal thread are maintained by redox poise emanating from built-in reducing reservoirs that restore oxidation-damaged Dopa (quinones and semi-quinones) back to Dopa and catecholato–metal bonds. Protein Cys thiols and Dopa provide this redox poise, but not as water-soluble antioxidants, because thiols in aqueous solution at pH ~7 are twice as oxidation-prone as Dopa. Instead, by sequestering thiols from Mfp6 and designated Dopa from Mfp3 within liquid–liquid phase-separated droplets or layers next to cohesively and adhesively challenged catecholato-metal ion protein scaffolds, controlled H^+ and e^- can be transferred as needed from droplets to damaged external quinones.

The H^+ and e^- transfers between coacervate droplets and external quinones ostensibly resemble miniaturized counterparts of membraneless quinone-based flow cell batteries[116,117]. However, the mechanisms by which thiols and catechols are stabilized within coacervates and the gating of droplet H^+ and e^- to external quinones remains speculative. For catechols, stabilization in coacervates is correlated with the formation of self–self bidentate H-bonds, whereas for thiols, S-σ-H···π-aromatic interactions have been proposed. Greater solute self–self H-bonding typically increases anodic redox potentials and is influenced by the solvent dielectric constant, which remains to be experimentally determined for coacervates. Field theoretical models of dense coacervate phases are unhelpful in this, assuming the dielectric constant to be the same as bulk water[101,102]. With respect to gating, we remain baffled. As coacervate droplets are membraneless, there is no option for channels or pumps. Probably, some sort of controllable H-bonding between internal catechols and external quinones exists at the coacervate–seawater interface. If the equilibrium within the droplets favours H-bonded dimers and trimers of catechols, an internal catechol will need a strong incentive to change partners. The H-bonds between catechols and *o*-quinones at synthetic interfaces are considerably stronger than those between paired catechols[109], which may provide this incentive. This and other questions require deeper investigations into the electronic properties of coacervate condensed matter.

The redox reservoirs of mussel byssus have useful insights to offer the next generation of sustainable high-performance adhesive polymers. Current research on bio-inspired, autonomous self-healing in conventional polymeric materials, including adhesives, is driven by three conceptual approaches: capsule-based healing, vascular-based healing and intrinsic healing[118]. In the first two approaches, hard-walled microcapsules or capillaries filled with liquid resin monomers and initiators are dispersed in a bulk matrix that is then cured and mechanically fractured. During crack formation, the walls of embedded crack-obstructing capsules or capillaries rupture, releasing their contents, resulting in local crack filling and repair. Notably, ruptured capsules cannot be used again. In intrinsic self-healing approaches, the polymer matrix is held together by unique reversible reactions and/or intermolecular interactions that rupture during crack formation and reform upon unloading[118,119].

Mussel byssus ostensibly takes advantage of all three self-healing approaches, though with notable differences. Byssal and synthetic platforms both depend on fluidic inclusions for self-healing, but the plaque droplets are unwalled and possess vascular interconnections with one-another by way of an open-pored structural mesh that enables extensive and intimate contact with the surrounding polymeric scaffold at all times. The intrinsic reversible interactions in plaque and cuticle are multivalent catecholato-metal ion complexes with stabilities ranked among the highest known[120] in coordination chemistry, with near-covalent bond energies. The situation in which byssus deviates most from manufactured materials is that its liquid inclusions are not crack-filling, but rather donate H^+ and e^- to repair the earliest stages of catechol oxidation, thereby iteratively restoring the intrinsic reformation of catecholato–metal interactions during crack self-repair. Possibly — unlike autonomous self-healing synthetic materials — nanotear formation in plaque and cuticle is an adaptive and purposeful device that enhances extension and toughness, but it requires diligent upkeep to counter oxidation and crack expansion. Such upkeep was not anticipated by applications such as the synthetic catecholato-Fe^{3+}-stabilized polymers prepared as hydrogels[8] or dry thermosets[9], hence resulted in serious material embrittlement after a few days.

A common sustainability rationale for synthetic self-healing materials is that extending the useful lifetime of a consumable material reduces the frequency of its replacement[119]. Self-healing synthetics that degrade into low-molecular-weight compounds upon obsolescence have been reported[121–123], and they advance our progress towards such materials by another notch. The catechol-based byssus improves upon self-healing materials even further by ultimately decomposing to components that support the renewal of the ambient ecosystem.

Published online: 15 January 2025

References

1. Wold, F. In vivo chemical modification of proteins (post-translational modification). *Annu. Rev. Biochem.* **50**, 738–814 (1981).
2. Waite, J. H. & Tanzer, M. L. Polyphenolic substance of *Mytilus edulis*: novel adhesive containing L-Dopa and hydroxyproline. *Science* **212**, 1038–1040 (1981).
3. Westerman, C. R., McGill, B. C. & Wilker, J. J. Sustainably sourced components to generate high-strength adhesives. *Nature* **621**, 306–311 (2023).
4. Shin, M. Complete prevention of blood loss with self-sealing haemostatic needles. *Nat. Mater.* **16**, 147–156 (2017).
5. Kim, E. et al. Graphene oxide/mussel foot protein composites for high strength and ultra-tough thin films. *Sci. Rep.* **10**, 19082 (2020).
6. Liu, Z. et al. Enhanced repairing of critical-sized calvarial bone defects by mussel-inspired calcium phosphate cement. *ACS Biomater. Sci. Eng.* **4**, 1852–1861 (2018).
7. Suárez-García, S., Nicotera, I., Ruiz-Molina, D. & Simari, C. A mussel-inspired coating for cost-effective and environmentally friendly CO_2 capture. *Chem. Eng. J.* **473**, 145280 (2023).
8. Holten-Andersen, N. et al. pH induced metal-ligand cross-links inspired by mussel yield self-healing polymer networks with near covalent elastic moduli. *Proc. Natl Acad. Sci. USA* **108**, 2651–2655 (2011).
The first report of a synthetic hydrogel cohesively held together by bis-catecholato-iron and tris-catecholato-iron complexes.
9. Filippidi, E. et al. Toughening elastomers using mussel-inspired iron-catechol complexes. *Science* **358**, 502–505 (2017).
Demonstration that catecholato-iron complexes can form in anhydrous polymers.
10. Maier, G. P., Bernt, C. M. & Butler, A. Catechol oxidation: considerations in the design of wet adhesive materials. *Biomater. Sci.* **6**, 332–339 (2018).
11. Menyo, M. S., Hawker, C. J. & Waite, J. H. Versatile tuning of supramolecular hydrogels through metal complexation of oxidation-resistant catechol-inspired ligands. *Soft Matter* **9**, 10314–10323 (2013).
12. Krogsgaard, M., Nue, V. & Birkedal, H. Mussel-inspired materials: self-healing through coordination chemistry. *Chem. Eur. J.* **22**, 844–857 (2016).
13. Krogsgaard, M., Hansen, M. R. & Birkedal, H. Metals & polymers in the mix: fine-tuning the mechanical properties & color of self-healing mussel-inspired hydrogels. *J. Mater. Chem. B* **2**, 8292–8297 (2016).
14. Lee, H., Scherer, N. F. & Messersmith, P. B. Single-molecule mechanics of mussel adhesion. *Proc. Natl Acad. Sci. USA* **103**, 12999–13003 (2006).
15. Waite, J. H. Mussel adhesion — essential footwork. *J. Exp. Biol.* **220**, 517–530 (2017).
16. Moeser, G. M. & Carrington, E. Seasonal variation in mussel byssal thread mechanics. *J. Exp. Biol.* **209**, 1996–2003 (2006).
17. Rising, A. & Harrington, M. J. Biological materials processing: time-tested tricks for sustainable fiber fabrication. *Chem. Rev.* **123**, 2155–2199 (2023).
18. Priemel, T. et al. Microfluidic-like fabrication of metal ion–cured bio-adhesives by mussels. *Science* **374**, 206–211 (2021).
This report examines how mussels traffic metals and Dopa prior to their interaction in byssus.
19. Roberts, E. A. et al. Resource allocation to a structural biomaterial: induced production of byssal threads decreases growth of a marine mussel. *Funct. Ecol.* **35**, 1222–1239 (2021).

20. Suchanek, T. H. The role of disturbance in the evolution of life history strategies in the intertidal mussels *Mytilus edulis* and *Mytilus californianus*. *Oecologia* **50**, 143–152 (1981).
21. Merkel, J. R., Dreisbach, J. H. & Ziegler, H. B. Collagenolytic activity of some marine bacteria. *Appl. Microbiol.* **29**, 145–151 (1975).
22. Wang, Y. et al. Structure of *Vibrio* collagenase VhaC provides insight into mechanism of bacterial collagenolysis. *Nat. Commun.* **13**, 566 (2022).
23. Cunha Neves, A., Harnedy-Rothwell, P. & FitzGerald, R. J. In vitro angiotensin-converting enzyme and dipeptidyl peptidase-IV inhibitory, and antioxidant activity of blue mussel (*Mytilus edulis*) byssus collagen hydrolysates. *Eur. Food Res. Technol.* **248**, 1721–1732 (2022).
24. Vogler, H. et al. The pollen tube: a soft shell with a hard core. *Plant. J.* **73**, 617–627 (2013).
25. Beaugendre, A. et al. Self-stratifying coatings: a review. *Prog. Org. Coat.* **110**, 210–241 (2017).
26. Sivasundarampillai, J. et al. A strong quick-release biointerface in mussels mediated by serotonergic cilia-based adhesion. *Science* **382**, 829–834 (2023).
The interface between byssus and living tissue has important implications for the design of prostheses.
27. Harrington, M. J., Masic, A., Holten-Andersen, N., Waite, J. H. & Fratzl, P. Iron-clad fibers: a metal-based biological strategy for hard flexible coatings. *Science* **328**, 216–220 (2010).
28. Schmitt, C. N. et al. Mechanical homeostasis of a DOPA-enriched biological coating from mussels in response to metal variation. *J. R. Soc. Interface* **12**, 0466 (2015).
29. Boerjan, W., Ralph, J. & Baucher, M. Lignin biosynthesis. *Annu. Rev. Plant Biol.* **54**, 519–546 (2003).
30. Johnstone, T. C. & Nolan, E. M. Determination of the molecular structures of ferric enterobactin and ferric enantioenterobactin using racemic crystallography. *J. Am. Chem. Soc.* **139**, 15245–15250 (2017).
31. Cao, W. et al. Unraveling the structure and function of melanin through synthesis. *J. Am. Chem. Soc.* **143**, 2622–2637 (2021).
32. Rubin, D. J., Miserez, A. & Waite, J. H. Diverse strategies of protein sclerotization in marine invertebrates: structure–property relationships in natural biomaterials. *Adv. Insect Physiol.* **38**, 75–133 (2010).
33. Saiz-Poseu, J., Mancebo-Aracil, J., Nador, F., Busqué, F. & Ruiz-Molina, D. The chemistry behind catechol-based adhesion. *Angew. Chem. Int. Ed.* **58**, 696–714 (2019).
An extensive overview of the versatile chemistry of catechols.
34. Andersen, A., Chen, Y. & Birkedal, H. Bioinspired metal–polyphenol materials: self-healing and beyond. *Biomimetics* **4**, 30 (2019).
35. Zhang, C. et al. Revisiting the adhesion mechanism of mussel-inspired chemistry. *Chem. Sci.* **13**, 1698–1705 (2022).
36. Yang, J., Cohen Stuart, M. A. & Kamperman, M. Jack of all trades: versatile catechol crosslinking mechanisms. *Chem. Soc. Rev.* **43**, 8271–8298 (2014).
37. Eslami, M., Zare, H. R. & Namazian, M. Thermodynamic parameters of electrochemical oxidation of L-DOPA: experimental and theoretical studies. *J. Phys. Chem. B* **116**, 12552–12557 (2012).
38. Segel, I. H. *Biochemical Calculations* 2nd edn (Wiley, 1976).
39. Proudfoot, G. M. & Ritchie, I. M. A cyclic voltammetric study of some 4-substituted benzene-1,2-diols. *Aust. J. Chem.* **36**, 885–894 (1989).
40. Moser, R. E. & Cassidy, H. G. Electron-transfer polymers. XXV. On "hydrophobic bonding." The effect of solvent on quinhydrone. *J. Am. Chem. Soc.* **87**, 3463–3467 (1965).
41. Li, G., Zhang, H., Sader, F., Vadhavkar, N. & Njus, D. Oxidation of 4-methylcatechol: implications for the oxidation of catecholamines. *Biochemistry* **46**, 6978–6983 (2007).
42. Wu, J. & Kozlowski, M. C. Catalytic oxidative coupling of phenols and related compounds. *ACS Catal.* **12**, 6532–6549 (2022).
43. Rodriguez, J., Contreras, D., Oviedo, C., Freer, J. & Baeza, J. Degradation of recalcitrant compounds by catechol-driven Fenton reaction. *Water Sci. Technol.* **49**, 81–84 (2004).
44. Song, H., Wignall, P. B., Song, H., Dai, X. & Chu, D. Seawater temperature and dissolved oxygen over the past 500 million years. *J. Earth Sci.* **30**, 236–243 (2019).
45. Miller, D. M., Buettner, G. R. & Aust, S. D. Transition metals as catalysts of "autoxidation" reactions. *Free Radic. Biol. Med.* **8**, 95–108 (1990).
46. Fass, D. & Thorpe, C. Chemistry and enzymology of disulfide cross-linking in proteins. *Chem. Rev.* **118**, 1169–1198 (2018).
Insightful review of the chemistry of thiols and disulfide formation.
47. Nicklisch, S. C. T., Spahn, J. E., Zhou, H., Gruian, C. M. & Waite, J. H. Redox capacity of an extracellular matrix protein associated with adhesion in *Mytilus californianus*. *Biochemistry* **55**, 2022–2030 (2016).
48. Martinez Rodriguez, N. R., Das, S., Kaufman, Y., Israelachvili, J. N. & Waite, J. H. Interfacial pH during mussel adhesive plaque formation. *Biofouling* **31**, 221–227 (2015).
49. Nakanishi, I. & Shoji, Y. Electrochemical redox behavior of 2,2-diphenyl-1-picrylhydrazyl radical solubilized by β-cyclodextrin in water. *Electrochem. Commun.* **134**, 107190 (2022).
50. Miller, D. R., Spahn, J. E. & Waite, J. H. Staying power of adhesion-associated antioxidant activity in *Mytilus californianus*. *J. R. Soc. Interface* **12**, 20150614 (2015).
51. Valois, E., Mirshafian, R. & Waite, J. H. Phase-dependent redox insulation in mussel adhesion. *Sci. Adv.* **6**, eaaz6486 (2020).
This report establishes the existence of Mfp3/Mfp6-containing reducing droplets in mussel plaques.
52. Zhao, H. & Waite, J. H. Linking adhesive and structural proteins in the attachment plaque of *Mytilus californianus*. *J. Biol. Chem.* **281**, 26150–26158 (2006).
53. DeMartini, D. G., Errico, J. M., Sjoestroem, S., Fenster, A. & Waite, J. H. A cohort of new adhesive proteins identified from transcriptomic analysis of mussel foot glands. *J. R. Soc. Interface* **14**, 20170151 (2017).
This is the first transcriptome for each of the byssal glands in *M. californianus*.
54. Farina, I. et al. High-performance Nylon-6 sustainable filaments for additive manufacturing. *Materials* **12**, 3955 (2019).
55. Harrington, M. J. & Waite, J. H. Holdfast heroics: comparing the molecular and mechanical properties of *Mytilus californianus* byssal threads. *J. Exp. Biol.* **210**, 4307–4318 (2007).
56. Carrington, E. & Gosline, J. M. Mechanical design of mussel byssus: load cycle and strain rate dependence. *Am. Malacol. Bull.* **18**, 135–142 (2004).
57. Waite, J. H., Holten Andersen, N., Jewhurst, S. & Sun, C. Mussel adhesion: finding the tricks worth mimicking. *J. Adhes.* **81**, 297–317 (2005).
58. Priemel, T. et al. Compartmentalized processing of catechols during mussel byssus fabrication determines the destiny of DOPA. *Proc. Natl Acad. Sci. USA* **117**, 7613–7621 (2020).
59. Bernstein, J. H., Filippidi, E., Waite, J. H. & Valentine, M. T. Effects of seawater pH on marine mussel plaque maturation. *Soft Matter* **16**, 9339–9346 (2020).
60. Hamada, N. A., Gilpin, C. & Wilker, J. J. Availability of environmental iron influences the performance of biological adhesives produced by blue mussels. *Environ. Sci. Technol.* **54**, 10254–10260 (2020).
61. Hwang, D. S. et al. Protein and metal-dependent interactions of a prominent protein in mussel adhesive plaques. *J. Biol. Chem.* **285**, 25850–25858 (2010).
62. Yang, B., Lim, C., Hwang, D. S. & Cha, H. J. Switch of surface adhesion to cohesion by Dopa-Fe^{3+} complexation, in response to microenvironment at the mussel plaque/substrate interface. *Chem. Mater.* **28**, 7982–7989 (2016).
63. Helm, C. A., Knoll, W. & Israelachvili, J. N. Measurement of ligand receptor interactions. *Proc. Natl Acad. Sci. USA* **88**, 8169–8173 (1991).
64. Papov, V. V., Diamond, T. V., Biemann, K. & Waite, J. H. Hydroxyarginine-containing polyphenolic proteins in the adhesive plaques of the marine mussel *Mytilus edulis*. *J. Biol. Chem.* **270**, 20183–20195 (1995).
65. Hwang, D. S. & Waite, J. H. Three intrinsically unstructured mussel adhesive proteins, mfp-1, mfp-2, and mfp-3: analysis by circular dichroism. *Protein Sci.* **21**, 1689–1695 (2012).
66. Waite, J. H. & Qin, X. X. Polyphosphoprotein from the adhesive pads of *Mytilus edulis*. *Biochemistry* **40**, 2887–2893 (2001).
67. Maier, G. P., Rapp, M. V., Waite, J. H., Israelachvili, J. N. & Butler, A. Adaptive synergy between catechol and lysine promotes wet adhesion by surface salt displacement. *Science* **349**, 628–632 (2015).
68. Cooper, L. H. N. Oxidation-reduction potential in seawater. *J. Mar. Biol. Assoc. UK* **22**, 167–176 (1937).
69. Qin, Z. & Buehler, M. Molecular mechanics of dihydroxyphenylalanine at a silica interface. *Appl. Phys. Lett.* **101**, 083702 (2012).
70. Danner, E. W., Kan, Y., Hammer, M. U., Israelachvili, J. N. & Waite, J. H. Adhesion of mussel foot protein Mefp-5 to mica: an underwater superglue. *Biochemistry* **51**, 6511–6518 (2012).
71. Yu, J. et al. Mussel protein adhesion depends on interprotein thiol-mediated redox modulation. *Nat. Chem. Biol.* **7**, 588–590 (2011).
72. Utzig, T., Stock, P. & Valtiner, M. Resolving non-specific and specific adhesive interactions of catechols at solid/liquid interfaces at the molecular scale. *Angew. Chem. Int. Ed.* **55**, 9524–9528 (2016).
73. Kan, Y., Danner, E. W., Israelachvili, J. N., Chen, Y. & Waite, J. H. Boronate complex formation with Dopa containing mussel adhesive protein retards pH-induced oxidation and enables adhesion to mica. *PLoS ONE* **9**, e108869 (2014).
74. Desmond, K. W., Zacchia, N. A., Waite, J. H. & Valentine, M. T. Dynamics of mussel plaque detachment. *Soft Matter* **11**, 6832–6839 (2015).
This study reports that the fracture energy of a single plaque is 6,000-fold greater than the adhesion energy of Mfp5.
75. Holten-Andersen, N., Fantner, G. F., Hohlbauch, S., Waite, J. H. & Zok, F. W. Protective coatings on extensible biofibres. *Nat. Mater.* **6**, 669–672 (2007).
76. Monnier, C. A., DeMartini, D. G. & Waite, J. H. Intertidal exposure favors the soft-studded armor of adaptive mussel coatings. *Nat. Commun.* **9**, 3424 (2018).
77. Waite, J. H. Evidence for a repeating 3, 4-dihydroxyphenylalanine- and hydroxyproline-containing decapeptide in the adhesive protein of the mussel, *Mytilus edulis* L. *J. Biol. Chem.* **258**, 2911–2915 (1983).
78. Taylor, S. W., Chase, D. B., Emptage, M. H., Nelson, M. J. & Waite, J. H. Ferric ion complexes of a DOPA-containing adhesive protein from *Mytilus edulis*. *Inorg. Chem.* **35**, 7572–7577 (1996).
79. Karpishin, T. B., Gebhard, M. S., Solomon, E. I. & Raymond, K. N. Spectroscopic studies of the electronic structure of iron(III) tris(catecholates). *J. Am. Chem. Soc.* **113**, 2977–2984 (1991).
80. Pierpont, C. G. & Buchanan, R. M. Transition metal complexes of *o*-benzoquinone, *o*-semiquinone, and catecholate ligands. *Coord. Chem. Rev.* **38**, 45–87 (1981).
81. Taylor, S. W., Luther, G. W. & Waite, J. H. Polarographic and spectrophotometric investigation of iron(III) complexation to 3, 4-dihydroxyphenylalanine-containing peptides and proteins from *Mytilus edulis*. *Inorg. Chem.* **33**, 5819–5824 (1994).
82. Waite, J. H., Tanzer, M. L. & Merkel, J. M. Nereis cuticle collagen. Proteolysis by marine vibrial and clostridial collagenases. *J. Biol. Chem.* **255**, 3596–3599 (1980).
83. Zeng, H., Hwang, D. S., Israelachvili, J. N. & Waite, J. H. Strong reversible Fe^{3+}-mediated bridging between dopa-containing protein films in water. *Proc. Natl Acad. Sci. USA* **107**, 12850–12853 (2010).
84. Xu, Z. Mechanics of metal catecholate complexes: the roles of coordination state and metal types. *Sci. Rep.* **3**, 2914 (2013).

85. Mesko, M. et al. Catechol-vanadium binding enhances cross-linking and mechanics of a mussel byssus coating protein. *Chem. Mater.* **33**, 6530–6540 (2021).
86. Menyo, M. S., Hawker, C. J. & Waite, J. H. Rate-dependent stiffness and recovery in interpenetrating network hydrogels through sacrificial metal coordination bonds. *ACS Macro Lett.* **4**, 1200–1204 (2015).
87. Valois, E., Hoffman, C., DeMartini, D. G. & Waite, J. H. The thiol-rich interlayer in the shell/core architecture of mussel byssal threads. *Langmuir* **35**, 15985–15991 (2019).
88. Inaba, K., Takahashi, Y.-H., Ito, K. & Hayashi, S. Critical role of a thiolate-quinone charge transfer complex and its adduct form in de novo disulfide bond generation by DsbB. *Proc. Natl Acad. Sci. USA* **103**, 287–292 (2005).
89. Ito, K. & Inaba, K. The disulfide bond formation (Dsb) system. *Curr. Opin. Struct. Biol.* **18**, 450–458 (2008).
90. George, M. N., Pedigo, B. & Carrington, E. Hypoxia weakens mussel attachment by interrupting DOPA cross-linking during adhesive plaque curing. *J. R. Soc. Interface* **15**, 20180489 (2018).
91. Hassenkam, T., Gutsmann, T., Hansma, P., Sagert, J. & Waite, J. H. Giant bent-core mesogens in the thread forming process of marine mussels. *Biomacromolecules* **5**, 1351–1355 (2004).
92. Qin, X. X., Coyne, K. J. & Waite, J. H. Tough tendons. Mussel byssus has collagen with silk-like domains. *J. Biol. Chem.* **272**, 32623–32627 (1997).
93. Sagert, J. & Waite, J. H. Hyperunstable matrix proteins in the byssus of *Mytilus galloprovincialis*. *J. Exp. Biol.* **212**, 2224–2236 (2009).
94. Merritt, M. E., Christensen, A. M., Kramer, K. J., Hopkins, T. L. & Schaefer, J. Detection of intercatechol cross-links in insect cuticle by solid-state carbon-13 and nitrogen-15 NMR. *J. Am. Chem. Soc.* **118**, 11278–11282 (1996).
95. Miserez, A., Rubin, D. & Waite, J. H. Cross-linking chemistry of squid beak. *J. Biol. Chem.* **285**, 38115–38124 (2010).
96. Liu, B., Burdine, L. & Kodadek, T. Chemistry of periodate-mediated cross-linking of 3, 4-dihydroxyphenylalanine-containing molecules to proteins. *J. Am. Chem. Soc.* **128**, 15228–15235 (2006).
Elegant demonstration that covalent cross-linking by *o*-dopaquinone works best in polymers when strategically aligned with nucleophiles.
97. Schmidt, S. et al. Metal-mediated molecular self-healing in histidine-rich mussel peptides. *Biomacromolecules* **15**, 1644–1652 (2014).
98. Kaim, W. & Schwederski, B. Non-innocent ligands in bioinorganic chemistry—an overview. *Coord. Chem. Rev.* **254**, 1580–1588 (2010).
99. Banerjee, R. Redox outside the box: linking extracellular redox remodeling with intracellular redox metabolism. *J. Biol. Chem.* **287**, 4397–4402 (2012).
100. Alberti, S., Gladfelter, A. & Mittag, T. Considerations and challenges in studying liquid-liquid phase separation and biomolecular condensates. *Cell* **176**, 419–434 (2019).
101. Li, L. et al. Phase behavior and salt partitioning in polyelectrolyte complex coacervates. *Macromolecules* **51**, 2988–2995 (2018).
102. Delaney, K. T. & Fredrickson, G. H. Theory of polyelectrolyte complexation — complex coacervates are self-coacervates. *J. Chem. Phys.* **146**, 224902 (2017).
103. Wei, W. et al. A mussel-derived one component adhesive coacervate. *Acta Biomater.* **10**, 1663–1670 (2014).
104. Wang, J. & Scheibel, T. Coacervation of the recombinant *Mytilus galloprovincialis* foot protein-3b. *Biomacromolecules* **19**, 3612–3619 (2018).
105. Deepankumar, K. et al. Liquid–liquid phase separation of the green mussel adhesive protein Pvfp-5 is regulated by the post-translated Dopa amino acid. *Adv. Mater.* **34**, 2103828 (2022).
Dopa in the byssus has multiple roles that go well beyond mussel adhesion.
106. Kaminker, I. et al. Simple peptide coacervates adapted for rapid pressure-sensitive wet adhesion. *Soft Matter* **13**, 9122–9131 (2017).
107. Yang, B., Jin, S., Park, Y., Jung, Y. M. & Cha, H. J. Coacervation of interfacial adhesive proteins for initial mussel adhesion to a wet surface. *Small* **14**, e1803377 (2018).
108. Kim, S. et al. Salt triggers the simple coacervation of an underwater adhesive when cations meet aromatic π electrons in seawater. *ACS Nano* **11**, 6764–6772 (2017).
First demonstration that cation–π interactions drive liquid–liquid phase separation of Mfp1 in seawater.
109. Ahn, B. K., Lee, D. W., Israelachvili, J. N. & Waite, J. H. Surface-initiated self-healing of polymers in aqueous media. *Nat. Mater.* **13**, 867–872 (2014).
110. Mirshafian, R., Wei, W., Israelachvili, J. N. & Waite, J. H. α,β-DehydroDopa: a hidden participant in mussel adhesion. *Biochemistry* **55**, 743–750 (2016).
111. Li, M. et al. Compliant clients: catechols exhibit enhanced solubility and stability in diverse complex coacervates. *Biomacromolecules* **24**, 4190–4198 (2023).
112. Papaefstathiou, G. S., Duncan, A. J. E. & MacGillivray, L. R. Two act as one: unexpected dimers of catechol direct a solid-state [2+2] photodimerization in a six-component hydrogen-bonded assembly. *Chem. Commun.* **50**, 15960–15962 (2014).
113. Ashizawa, R. & Noguchi, T. Effects of hydrogen bonding interactions on the redox potential and molecular vibrations of plastoquinone as studied using density functional theory calculations. *Phys. Chem. Chem. Phys.* **16**, 11864–11876 (2014).
114. Forbes, C. R. et al. Insights into thiol–aromatic interactions: a stereo-electronic basis for S–H/π interactions. *J. Am. Chem. Soc.* **139**, 1842–1855 (2017).
115. Kim, H. et al. Essential role of thiols in maintaining stable catecholato-iron complexes in condensed materials. *Chem. Mater.* **34**, 5074–5083 (2022).
116. Yurko, Y. & Elbaz, L. Direct quinone fuel cells. *J. Am. Chem. Soc.* **145**, 2653–2660 (2023).
117. Leung, P. K., Martin, T., Shah, A. A., Anderson, M. A. & Palma, J. Membrane-less organic–inorganic aqueous flow batteries with improved cell potential. *Chem. Commun.* **52**, 14270–14273 (2016).
118. Blaizik, B. J. et al. Self-healing polymers and composites. *Annu. Rev. Mater. Res.* **40**, 179–211 (2010).
119. Choi, K. et al. Properties and applications of self-healing polymeric materials: a review. *Polymers* **15**, 4408 (2023).
120. Sillén, L. G. *Stability Constants of Metal-ion Complexes* (Chemical Society, 1964).
121. Tong, L. et al. A new self-healing degradable copolymer based on polylactide and poly(p-dioxanone). *Molecules* **28**, 4021 (2023).
122. Chen, R. et al. A self-healable, recyclable and degradable soft network structure material for soft robotics. *Mater. Des.* **227**, 111783 (2023).
123. Agergaard, A. H., Sommerfeldt, A., Pedersen, S. U., Birkedal, H. & Daasbjerg, K. Dual-responsive material based on catechol-modified self-immolative poly(disulfide) backbones. *Angew. Chem. Int. Ed.* **60**, 21543–21549 (2021).
124. Liu, L.-M., Li, S.-C., Cheng, H., Diebold, U. & Selloni, A. Growth and organization of an organic molecular monolayer on TiO_2: catechol on anatase (101). *J. Am. Chem. Soc.* **133**, 7816–7823 (2011).
125. Waite, J. H. The catechol oxidase in the byssus of the common mussel, *Mytilus edulis* L. *J. Mar. Biol. Assoc. UK* **65**, 359–371 (1985).

Acknowledgements

The authors acknowledge the many inspired colleagues and trainees who worked to bring mussel byssus biochemistry to its present state. This work was supported by a National Science Foundation Materials Research Science & Engineering Center Grant [DMR 1720256].

Author contributions

S.X.W. and J.H.W. researched and critiqued the literature and wrote the Review.

Competing interests

The authors declare no competing interests.

Additional information

Peer review information *Nature Reviews Chemistry* thanks Henrik Birkedal, Qiang Wei and the other, anonymous, reviewer(s) for their contribution to the peer review of this work.